REPORT DOCUMENTATION PAGE

1. REPORT DATE *(DD-MM-YYYY)*	2. REPORT TYPE	3. DATES COVERED *(From - To)*
02-28-2010	FINAL TECHNICAL	June 1, 2008 - May 31, 2009

4. TITLE AND SUBTITLE
LWIR Microgrid Polarimeter for Remote Sensing Studies

5a. CONTRACT NUMBER

5b. GRANT NUMBER
FA9550-08-1-0295

5c. PROGRAM ELEMENT NUMBER

6. AUTHOR(S)
J. Scott Tyo

5d. PROJECT NUMBER

5e. TASK NUMBER

5f. WORK UNIT NUMBER

7. PERFORMING ORGANIZATION NAME(S) AND ADDRESS(ES)
College of Optical Sciences
University of Arizona
1630 E University Blvd.
Tucson, AZ 85721

8. PERFORMING ORGANIZATION REPORT NUMBER

9. SPONSORING/MONITORING AGENCY NAME(S) AND ADDRESS(ES)
AFOSR/NE
875 N. Randolph, Ste.325, Rm. 3112,
Arlington Virginia, 22203

10. SPONSOR/MONITOR'S ACRONYM(S)
AFOSR/NE

11. SPONSOR/MONITOR'S REPORT NUMBER(S)

12. DISTRIBUTION/AVAILABILITY STATEMENT
Unlimited

13. SUPPLEMENTARY NOTES

14. ABSTRACT
A LWIR microgrid polarimeter was integrated under this DURIP proposal. The FPA was a HgCdTe 640 x 480 array from DRS with an integrated micropolarizer array. The camera was integrated by SE-IR in Santa Barbara, CA. The system was calibrated and tested at the University of Arizona, and preliminary images are shown in this final report.

15. SUBJECT TERMS
Remote Sensing, polarimetry

16. SECURITY CLASSIFICATION OF:			17. LIMITATION OF ABSTRACT	18. NUMBER OF PAGES	19a. NAME OF RESPONSIBLE PERSON
a. REPORT	b. ABSTRACT	c. THIS PAGE			J. Scott Tyo
U	U	U	Unlimited	7	19b. TELEPHONE NUMBER *(Include area code)* 520-626-8183

# LWIR Microgrid Polarimeter for Remote Sensing Studies

J. Scott Tyo

College of Optical Sciences
University of Arizona
Tucson, AZ, 85721
tyo@optics.arizona.edu

Under this DURIP program, we designed, procured, and integrated a LWIR microgrid polarimeter. In addition, we performed initial training, calibration, and verification on the camera system. Multiple intensity measurements are required to determine the polarization state of light.[1] These multiple measurements can be made sequentially in time using a single detector (or array of detectors for imaging polarimetry), or they can be made simultaneously using several detector arrays located at different physical positions. Numerous strategies have been developed to affect the simultaneous measurements, as discussed in a recent review article.[2]

One approach that has been developed for rapid acquisition of polarimetric data is to place polarization filters directly on individual detector elements of the FPA.[3] This advanced FPA technology allows simultaneous collection of data sets associated with each of the polarizer orientations in the array. The specific instrument that we are working with is a 640 x 480, engineering-grade, HgCdTe FPA manufactured by DRS Sensors and Targeting Systems operating in the band 8–10 μm. The FPA has an integrated wire grid polarizer array that is aligned and bonded to the FPA.[4] The polarizer arrangement forms an alternating pattern of 0, 45, 90, and 135 degree orientations as shown in Fig. 1, and the measured intensity data is processed to estimate the first three (s_0, s_1, s_2) Stokes parameters.[5] In principle only three measurements are necessary, but the fourth measurement provides robustness, reduces noise, aids in eliminating the effects of dead pixels in the FPA[6] and fits well with the rectangular nature of the FPA pixel pattern.[7–9] The polarization estimate is reconstructed at the intersection of the four pixels that compose a single sub-quad of pixels or a "super pixel" as depicted in Fig. 2 using one of several interpolation strategies.[10] These polarized FPAs allow for direct replacement of existing thermal FPAs, augmenting the thermal imagery by providing additional information in real time.

The FPA was purchased from DRS Sensors and Targeting Systems. The cooler was purchased from L3 Technologies (Cincinnati Electronics). The system was integrated by SE-IR in Santa Barbara, CA. We are using a Janos F/2, 50-mm-focal length LWIR lens, and we have integrated a band-pass filter with a pass band of 7.9 - 9.9 microns.
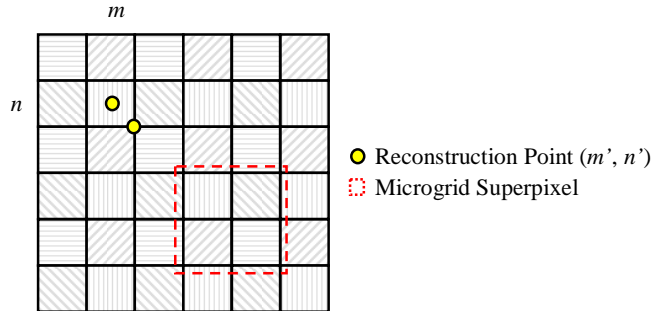
Figure 1. Division of Focal Plane (DoFP) polarimeters operate by placing a micropolarizer in front of each pixel that analyzes a different polarization state. Stokes vectors are estimated at interpolation points as shown in the figure.[4]
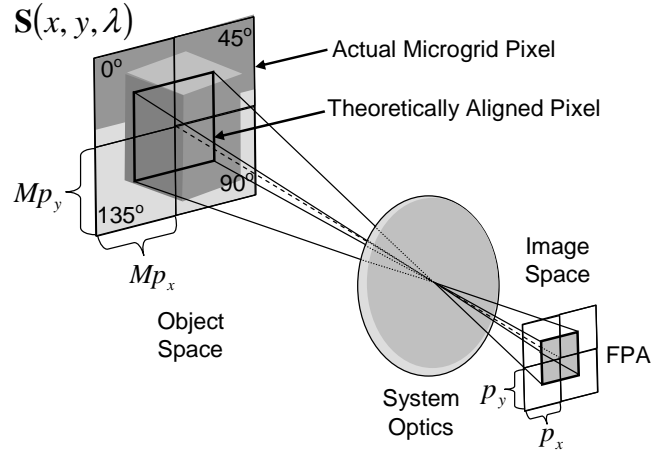
Figure 2. Super-pixel of the microgrid polarimeter.

Figure 3. LWIR microgrid camera (center) with the control electronics (right) being calibrated with a blackbody (blue box on left).

the SE-IR system came with their CAM-IRA software package. We use Cam-IRA for diagnostics and testing, but we have also written our own custom libraries that we use for experimentation and data collections. The camera system was integrated onto a portable workstation so it could be taken out of the lab for testing. The camera is shown in our laboratory in Fig. 3.

Example polarimetric imagery taken both inside the lab and outside the lab are shown in Fig. 4. A recently published paper from *Optics Letters* it appended to this report as Appendix A that includes data taken with the DURIP polarimeter.

Figure 4. Left: Image of a warm emissive sphere taken in our laboratory at the College of Optical Sciences. Right; Image of the Flandrau Science Center on the campus of the University of Arizona. Taken from the roof of the Meinel Building, College of Optical Sciences.

REFERENCES

1. R. A. Chipman, "Polarimetry," in *Handbook of Optics*, M. Bass, ed., vol. 2, ch. 22, McGraw-Hill, 1995.
2. J. S. Tyo, D. H. Goldstein, D. B. Chenault, and J. A. Shaw, "Review of passive imaging polarimetry for remote sensing applications," *Appl. Opt.* **45**, pp. 5453 – 5469, August 2006.
3. A. G. Andreou and Z. K. Kalayjian, "Polarization imaging: principles and integrated polarimeters," *IEEE Sens. J.* **2**, pp. 566 – 576, 2002.
4. D. L. Bowers, J. K. Boger, L. D. Wellems, W. T. Black, S. E. Ortega, B. M. Ratliff, M. P. Fetrow, J. E. Hubbs, and J. S. Tyo, "Evaluation and display of polarimetric image data using long-wave cooled microgrid focal plane arrays," in *Proc. SPIE vol. 6240: Polarization: Measurement, Analysis, and Remote Sensing VII*, D. H. Goldstein and D. B. Chenault, eds., p. 6240OF, SPIE, (Bellingham, WA), 2006.
5. R. M. A. Azzam and N. M. Bashara, *Ellipsometry and Polarized Light*, North-Holland, New York, 1977.
6. B. M. Ratliff, J. S. Tyo, J. K. Boger, W. T. Black, D. L. Bowers, and M. P. Fetrow, "Dead pixel replacement in lwir microgrid polarimeters," *Opt. Express* **15**, pp. 7596 – 7609, 2007.
7. R. Walraven, "Polarization imagery," *Opt. Eng.* **20**, pp. 14 – 18, 1981.
8. J. S. Tyo, "Optimum linear combination strategy for a N-channel polarization sensitive vision or imaging system," *J. Opt. Soc. Am. A* **15**, pp. 359–366, 1998.
9. J. S. Tyo, "Design of optimal polarimeters: maximization of SNR and minimization of systematic errors," *Appl. Opt.* **41**, pp. 619–630, 2002.
10. B. M. Ratliff, J. K. Boger, M. P. Fetrow, J. S. Tyo, and W. T. Black, "Image processing methods to compensate for ifov errors in microgrid imaging polarimeters," in *Proc. SPIE vol. 6240: Polarization: Measurement, Analysis, and Remote Sensing VII*, D. H. Goldstein and D. B. Chenault, eds., p. 6240OE, SPIE, Bellingham, WA, 2006.

Total elimination of sampling errors in polarization imagery obtained with integrated microgrid polarimeters

J. Scott Tyo,* Charles F. LaCasse, and Bradley M. Ratliff

College of Optical Sciences, University of Arizona, 1630 East University Boulevard, Tucson, Arizona 85721, USA
*Corresponding author: tyo@ieee.org

Microgrid polarimeters operate by integrating a focal plane array with an array of micropolarizers. The Stokes parameters are estimated by comparing polarization measurements from pixels in a neighborhood around the point of interest. The main drawback is that the measurements used to estimate the Stokes vector are made at different locations, leading to a false polarization signature owing to instantaneous field-of-view (IFOV) errors. We demonstrate for the first time, to our knowledge, that spatially band limited polarization images can be ideally reconstructed with no IFOV error by using a linear system framework. © 2009 Optical Society of America

OCIS codes: 110.5405, 120.2130, 120.5410.

Recent years have seen the emergence of passive polarimetric imagery as an important discriminating tool in many areas of sensing. Polarization has been used to help in target detection, defeat clutter, and see through mildly turbid media, among other applications. A recent review paper [1] contains an in-depth discussion of many of these applications.

Polarized incoherent light is often described in terms of the Stokes vector,

$$\mathbf{S} = [s_0 \ s_1 \ s_2 \ s_3]^T$$
$$= [I_H + I_V \ I_H - I_V \ I_{45} - I_{135} \ I_L - I_R]^T, \quad (1)$$

where I_H, I_V, I_{45}, I_{135}, I_L, and I_R are the intensities observed through horizontal, vertical, 45°, 135°, left-circular, and right-circular polarizers, respectively. Microgrid polarimeters combine an array of micropolarizers with a focal plane array (FPA) to make a spatially modulated measurement of the polarized intensity [2]. The most common configuration is as shown in Fig. 1, where four linear polarization states are interlaced to estimate the three linear polarization Stokes parameters s_0, s_1, and s_2. However, systems have been proposed where other polarization measurements are made, including full polarimeters that also measure the circularly polarized component [3,4].

Microgrid polarimeters are attractive because they are rugged and inherently optomechanically aligned. The largest drawback of these systems is that the Stokes parameters are estimated using polarization measurements from different locations in the FPA. When there are intensity variations in addition to polarization variations across the scene, the different instantaneous fields of view (IFOVs) of neighboring pixels complicate the reconstruction process and are the primary source of false polarization signatures [5].

All studies known to us reconstruct the polarization estimates from the raw microgrid image by using spatially local interpolation kernels [1,2,4,6,7]. A recent study demonstrated that the false polarization signatures in these cases are because of an incomplete demodulation of the intensity image [5].

Microgrid polarimeters are a class of "snapshot" polarimeters that determine all of the desired polarization information from a single measurement of intensity on a single FPA. Prismatic polarimeters [8–10] are another class of snapshot polarimeter that use two spatially varying multiorder wave plates (birefringent prisms) to introduce polarization-dependent carrier fringes that are modulated by the image intensity, thereby creating polarization-dependent sidebands in the spatial frequency plane. Comparing the results of Ratliff *et al.* [5] for microgrid instruments to those from prismatic polarimeters led us to the present Letter, which uses a linear system framework to create ideal microgrid interpolation kernels that can perfectly reconstruct band limited polarization imagery.

We develop the theory here for the specific configuration shown in Fig. 1; however, the theory is easy to extend to an arbitrary micropolarizer layout. We will assume that the pixels in the FPA are ideal point samplers; the effects of finite pixel size and shape can be included using the standard sampling theory. The image is described by the spatially varying Stokes
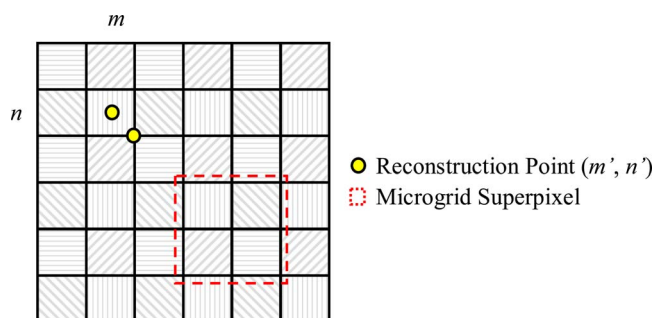

Fig. 1. (Color online) Typical microgrid polarimeter uses four interlaced linear polarizer orientations to estimate s_0, s_1, and s_2.

vector image $\mathbf{S}_i(m,n)$. The intensity measured by the (m,n)th pixel can be written as

$$I(m,n) = \mathbf{S}_A(m,n)^T \cdot \mathbf{S}_i(m,n), \qquad (2)$$

where $\mathbf{S}_A(m,n)$ is the analyzer Stokes vector of the (m,n)th pixel that is expressed as

$$\mathbf{S}_A = (m,n)\begin{bmatrix} 1 \\ \frac{1}{2}(\cos(m\pi) + \cos(n\pi)) \\ \frac{1}{2}(\cos(m\pi) - \cos(n\pi)) \\ 0 \end{bmatrix}. \qquad (3)$$

Substituting Eq. (3) into Eq. (2) yields

$$I(m,n) = s_0(m,n) + \tfrac{1}{2}\cos(m\pi)[s_1(m,n) + s_2(m,n)]$$
$$+ \tfrac{1}{2}\cos(n\pi)[s_1(m,n) - s_2(m,n)]. \qquad (4)$$

Next we take the discrete-space Fourier transform (DSFT) of $I(m,n)$. We assume that the Stokes parameter images are spatially band limited enough to avoid aliasing (this condition will be made explicit below), and we consider only the positive frequencies as

$$\tilde{I}(\xi,\eta) = \tilde{S}_0(\xi,\eta) + \tfrac{1}{4}\left[\tilde{S}_1\left(\xi - \tfrac{1}{2}, \eta\right) + \tilde{S}_2\left(\xi - \tfrac{1}{2}, \eta\right)\right]$$
$$+ \tfrac{1}{4}\left[\tilde{S}_1\left(\xi, \eta - \tfrac{1}{2}\right) - \tilde{S}_2\left(\xi, \eta - \tfrac{1}{2}\right)\right], \qquad (5)$$

where ξ and η are the horizontal and the vertical spatial frequencies (in cycles per pixel), respectively. In Eq. (5) there is a baseband signal carrying s_0, a horizontal sideband signal at $\xi = \tfrac{1}{2}$ that represents $s_1 + s_2$, and a vertical sideband at $\eta = \tfrac{1}{2}$ that represents $s_1 - s_2$.

To demonstrate an ideal reconstruction we use the simple polarized scene described by

$$s_0(n,m) = e^{-36(n^2 + m^2)}, \qquad (6)$$

$$s_1(n,m) = \tfrac{1}{2}s_0(n,m)\mathrm{erf}(2m), \qquad (7)$$

$$s_2(n,m) = \tfrac{1}{2}s_0(n,m)\mathrm{erf}(2n). \qquad (8)$$

The Fourier transform of $I(m,n)$ for this excitation is shown in Fig. 2. We see both the baseband signal that corresponds to the Fourier transform of s_0 and the horizontal and the vertical sidebands predicted in Eq. (5).

We can use Fig. 2 to form a quantitative description of the band limit requirements. There are many ways that the spatial frequency information among s_0, s_1, and s_2 can be distributed to allow a perfect reconstruction. However, if we assume that s_0 is spatially band limited to $\sqrt{\xi^2 + \eta^2} < W_0$ and s_1 and s_2 are spatially band limited to $\sqrt{\xi^2 + \eta^2} < W_1$, a sufficient condition to avoid aliasing is that $W_0 + W_1 < \tfrac{1}{2}$.

The reconstruction errors for s_0 and s_1 using the filters indicated in Fig. 2 are shown in Fig. 3 for our method (Fig. 3A) and the standard nearest like-polarization neighbor (NLPN) interpolation strategy (Fig. 3B). The NLPN method reconstructs the Stokes vector estimates at each node in Fig. 1 using the four
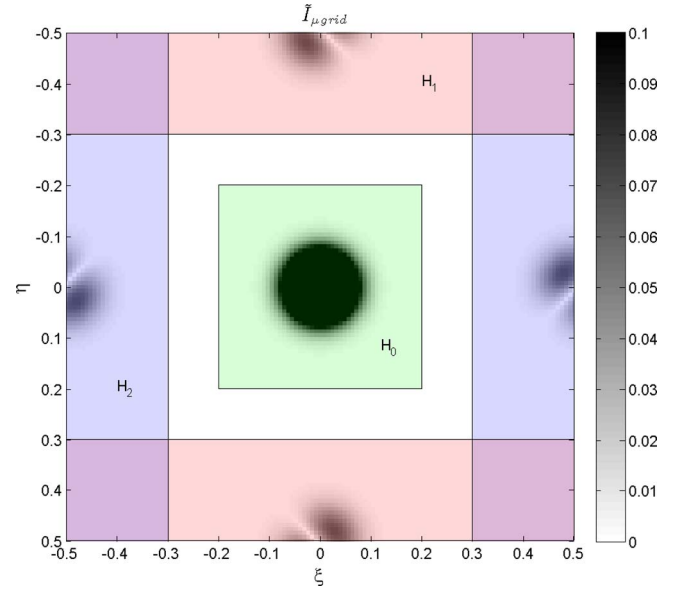

Fig. 2. (Color online) Fourier transform of $I(m,n)$ for the excitation defined by Eqs. (6)–(8). The outer shaded regions represent the high-pass filters used to reconstruct s_1 and s_2. The central shaded area is the low-pass filter used to reconstruct s_0.

pixels that contact that node [5]. The NLPN interpolation is the most widely used reconstruction method for microgrid polarimeters [2,4,6,7].

The general notion in the polarization imaging community is that the NLPN interpolation can be used to create good reconstructions by simply choosing the point spread function of the optics to band limit the image. A second notion is that microgrid polarimeters can only reconstruct accurately scenes that have features that are constant across a single 4×4 superpixel. Figure 3 clearly demonstrates that these notions are false. What error is present in Figs. 3A and 3B is because the images defined in Eqs. (6)–(8) are not in fact band limited, resulting in small aliasing effects. Other more complicated interpola-
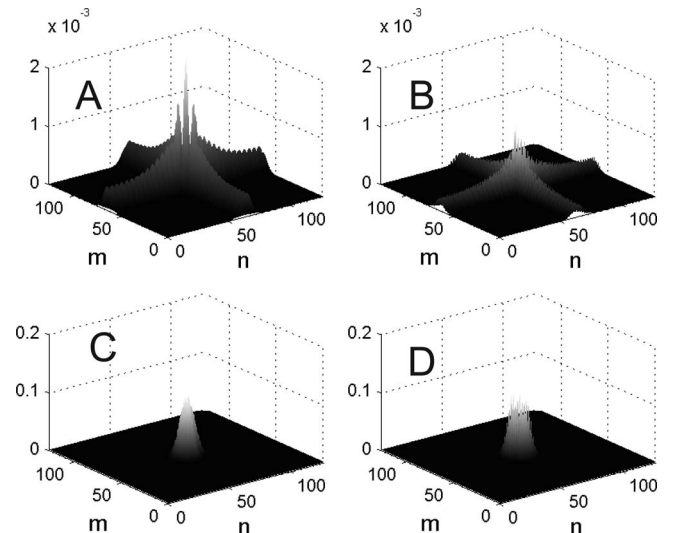

Fig. 3. s_0 (left column) and s_1 (right column) error distributions for the ideal reconstruction strategy presented here (top row) and NLPN interpolation (bottom row).

tors than the NLPN method can do a better job of reconstructing the polarization information than the NLPN [5], but the improvement in those cases is by less than 1 order of magnitude (data not shown). This occurs because the interpolation kernel for the NLPN is a 2×2 rectangular window. This interpolation kernel will have a corresponding sinc-function filter in the frequency domain that allows significant spectral leakage of the sidelobe signals into the reconstructed baseband signal, and vice versa. This can be interpreted as a form of polarimetric aliasing.

A comparison between the NLPN and the linear system method presented here is shown for real data in Fig. 4. The object here is a 45 cm diameter brass sphere painted with krylon flat black paint and heated with an incandescent light bulb to 50°C. The sphere is located in a laboratory with a nominal room temperature of 23°C. It is expected that the predominant polarization signature around the sphere will be p polarized, since the emitted radiation dominates the image. The degree of polarization is expected to be maximal near the edges where the photons leave the sphere near grazing, and the degree of polarization near the center of the sphere should be approximately zero. Figures 4C and 4D are colored using a transform that maps the angle of polarization into color hue and the degree of linear polarization into color saturation [11]. To mitigate the effects of aliasing we used Hamming windows for our frequency domain filters.

Microgrid polarimetric imagers were an extremely popular area of research owing to their ruggedness

and inherent optomechanical alignment, but they lost favor because of the polarimetric aliasing problems near contrast edges in images apparent in Fig. 4D. In this Letter we have presented a reconstruction paradigm that eliminates these artifacts, making microgrid instruments competitive with other polarimetric modalities [1]. By operating in the frequency domain, it is possible to perfectly reconstruct spatially band limited polarization scenes with no IFOV error for the first time known to the authors. In certain instances it might be preferable to perform the reconstruction without taking a Fourier transform. For example, several researchers have developed methods to perform the polarimetric reconstruction in hardware at the FPA by making local arithmetic computations [2,6]. The results derived here can be used to derive spatially local interpolation kernels that have greatly improved error performance over the methods currently employed [5]. Finally, going to the frequency domain allows us to consider the application of superresolution methods that can exploit aliasing to improve the resolution beyond the superpixel or even individual pixel levels. This is an active area of current work [13].

Fig. 4. (Color online) Long-wave IR (8–10 μm) polarimetric imagery taken using a microgrid polarimeter described elsewhere [12]. The target is a spherical gray body at 50°C. A, Calibrated microgrid image with modulation present. B, Fourier transform of $I(m,n)$. C, Reconstruction using Eq. (5). D, Reconstruction using NLPN interpolation [5].

References

1. J. S. Tyo, D. H. Goldstein, D. B. Chenault, and J. A. Shaw, Appl. Opt. **45**, 5453 (2006).
2. A. G. Andreou and Z. K. Kalayjian, IEEE Sens. J. **2**, 566 (2002).
3. G. P. Nordin, J. T. Meier, P. C. Deguzman, and M. Jones, Proc. SPIE **3754**, 169 (1999).
4. C. K. Harnett and H. G. Craighead, Appl. Opt. **41**, 1291 (2002).
5. B. M. Ratliff, C. F. Lacasse, and J. S. Tyo, Opt. Express **17**, 9112 (2009).
6. V. Gruev, K. Wu, J. V. der Spiegel, and N. Engheta, Proc. SPIE **6240**, 6240O5 (2006).
7. C. S. L. Chun, D. L. Fleming, and E. J. Torok, Proc. SPIE **2234**, 275 (1994).
8. K. Oka and T. Kaneko, Opt. Express **11**, 1510 (2003).
9. H. Luo, K. Oka, N. Hagen, T. Tkaczyk, and E. L. Dereniak, Appl. Opt. **45**, 8400 (2006).
10. M. W. Kudenov, L. Pezzaniti, E. L. Dereniak, and G. R. Gerhart, Opt. Express **16**, 13720 (2008).
11. J. S. Tyo, E. N. Pugh, and N. Engheta, J. Opt. Soc. Am. A **15**, 367 (1998).
12. D. L. Bowers, J. K. Boger, L. D. Wellems, S. E. Ortega, M. P. Fetrow, J. E. Hubbs, W. T. Black, B. M. Ratliff, and J. S. Tyo, Opt. Eng. **47**, 046403 (2008).
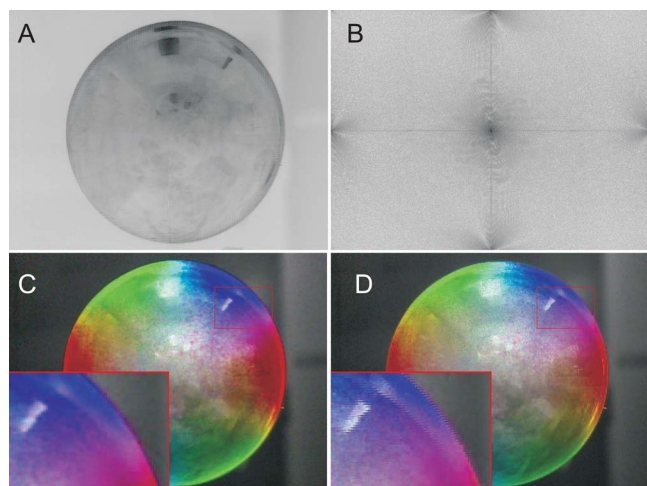13. B. M. Ratliff, J. S. Tyo, C. F. LaCasse, and W. T. Black, Proc. SPIE **7461**, 74610K (2009).